Asian Journal of Pharmaceutical Sciences 18 (2023) 100827

Available online at www.sciencedirect.com

ScienceDirect

journal homepage: www.elsevier.com/locate/AJPS

Original Research Paper

Phytoestrogen-derived multifunctional ligands for targeted therapy of breast cancer ☆

Ying Zhang [a,b,1], *Hao Pan* [c,1], *Changxiang Yu* [a,b], *Rui Liu* [a,b], *Bin Xing* [a,b], *Bei Jia* [a,b], *Jiachen He* [a,b], *Xintao Jia* [a,b], *Xiaojiao Feng* [a,b], *Qingqing Zhang* [a,b], *Wenli Dang* [a,b], *Zheming Hu* [a,b], *Xiuping Deng* [a,b], *Pan Guo* [a,b], *Zhidong Liu* [a,b,*], *Weisan Pan* [d,*]

[a] *State Key Laboratory of Component-based Chinese Medicine, Tianjin University of Traditional Chinese Medicine, Tianjin 301617, China*
[b] *Ministry of Education, Tianjin University of Traditional Chinese Medicine, Tianjin 301617, China*
[c] *School of Pharmacy, Liaoning University, Shenyang 110036, China*
[d] *School of Pharmacy, Shenyang Pharmaceutical University, Shenyang 110016, China*

ARTICLE INFO

Article history:
Received 19 January 2023
Revised 20 April 2023
Accepted 31 May 2023
Available online 7 July 2023

Keywords:
Phytoestrogen
Tanshinone IIA
Doxorubicin
Breast cancer
Targeting delivery

ABSTRACT

Nano-targeted delivery systems have been widely used for breast tumor drug delivery. Estrogen receptors are considered to be significant drug delivery target receptors due to their overexpression in a variety of tumor cells. However, targeted ligands have a significant impact on the safety and effectiveness of active delivery systems, limiting the clinical transformation of nanoparticles. Phytoestrogens have shown good biosafety characteristics and some affinity with the estrogen receptor. In the present study, molecular docking was used to select tanshinone IIA (Tan IIA) among phytoestrogens as a target ligand to be used in nanodelivery systems with some modifications. Modified Tan IIA (Tan-NH_2) showed a good biosafety profile and demonstrated tumor-targeting, anti-tumor and anti-tumor metastasis effects. Moreover, the ligand was utilized with the anti-tumor drug Dox-loaded mesoporous silica nanoparticles via chemical modification to generate a nanocomposite Tan-Dox-MSN. Tan-Dox-MSN had a uniform particle size, good dispersibility and high drug loading capacity. Validation experiments *in vivo* and *in vitro* showed that it also had a better targeting ability, anti-tumor effect and lower toxicity in normal organs. These results supported the idea that phytoestrogens with high affinity for the estrogen receptor could improve the therapeutic efficacy of nano-targeted delivery systems in breast tumors.

☆ Peer review under responsibility of Shenyang Pharmaceutical University.

* Corresponding authors.
E-mail addresses: liuzhidong@tjutcm.edu.cn (Z. Liu), ppwwss@163.com (W. Pan).

[1] These authors contributed equally to this work.
Peer review under responsibility of Shenyang Pharmaceutical University.

https://doi.org/10.1016/j.ajps.2023.100827

1. Introduction

Breast cancer threatens human health worldwide, and personalized drug delivery is a promising strategy for cancer treatment. According to the latest cancer statistics released in 2022, breast cancer accounted for 31% of new cancer cases in American women, with an estimated mortality rate of 15% [1]. The rapid development of nanotechnology has improved the delivery of tumor drugs and reduced the side effects of anticancer drugs while increasing their efficacy [2]. Many researchers use the enhanced permeability and retention (EPR) effect to achieve the good targeting effect of nanodrugs through passive targeting and accordingly improve the drug efficacy; however, the performance of passive targeting research results in clinical translation is not ideal. The main reason is that in normal tissues, nanoparticles cannot easily penetrate the capillary wall with intact structure and dense endothelial space [3].

Active targeting strategies can target the tumor tissue more specifically than passive targeting using the EPR effect alone. In recent years, various targeted ligands have been applied to active targeted delivery, such as hyaluronic acid [4], angiopep-2 [5], p32 and Her2-specific ligand [6,7], which achieving good therapeutic effects on breast cancer brain metastases. Currently, active targeting nanoparticles are internalized through receptor-mediated endocytosis, and their cellular uptake is much higher than that of unmodified nanoparticles, resulting in better therapeutic effects [8]. Clinical studies have shown that in breast cancer tissue, the estrogen receptor (ER) positively correlated with the tumor size and is involved in tumor metastasis [9]. In estrogen-dependent breast cancer, ER is expressed in 70%–80% breast cancer cells but in only 15%–25% normal breast cells. Several clinical experiments have confirmed that ERs are overexpressed in endometrial cancer, laryngeal cancer, ovarian cancer, lung cancer and other tissues [10–13]. At present, various nanodelivery systems targeting ERs have been developed, and the targeting ligands used mainly include estradiol [14], estrone [15], tamoxifen [16] and endoxifen [17]. Among them, estradiol and estrone have a higher affinity to the receptors; however, estrone was reported to have a risk of promoting breast cancer proliferation and metastasis [18].

To screen novel targeted ligands, molecular docking technology is widely used to reveal the interaction between structurally determined receptors and preselected ligands [19,20]. Phytoestrogen is a kind of natural product with a structure and function similar to those of estrogen. Phytoestrogens and breast cancer are closely related [21–23]. In a recent study, researchers evaluated the chemosensitization and apoptotic effect of phytoestrogens on breast cancer cells with molecular docking prediction and *in vitro* studies [24]. The phytoestrogens show potent activity on breast cell lines. Based on this, we hypothesized that phytoestrogens as ligands can effectively bind to ERs or breast cancer tissues and avoid the risk of promoting tumor cell proliferation and metastasis.

In this study, we evaluated the binding effect of phytoestrogens with antitumor activity (Fig. 1) on ER by molecular docking. As the main active ingredient of *Salvia miltiorrhiza* [25], tanshinone IIA (Tan IIA) was selected from phytoestrogens by the molecular docking method as a target ligand and used in nanodelivery systems with modification (Tan-NH_2). Moreover, Tan-NH_2 was grafted onto mesoporous silica nanoparticles (MSNs) to prepare targeted functional nanoparticles (Tan-MSN) and encapsulated doxorubicin hydrochloride (Dox) in MSNs as a model drug. Physicochemical characterization and hemolysis safety research were carried out on the Tan IIA-modified MSN loaded with Dox (Tan-Dox-MSN), and the *in vitro* and *in vivo* targeting ability, antitumor efficacy and safety of Tan-Dox-MSN were assessed.

2. Materials and method

2.1. Materials

Tan IIA, indocyanine green (ICG) and glycine ethyl ester hydrochloride were obtained from Shanghai Yuanye Bio-Technology Co., Ltd. (Shanghai, China). Dox with >98% purity was obtained from Dalian Meilun Bio-Technology Co., Ltd. (Dalian, China). Human breast carcinoma cells (MCF-7, T47D), human breast cells (MCF10A) and complete growth medium (Catalog No.: SCSP-660) for MCF10A cells were acquired from the National Collection of Authenticated Cell Cultures (Shanghai, China). These cells were cultivated in minimum essential medium (MEM; Gibco, 89% for MCF-7) or Dulbecco's Modified Eagle's Medium (DMEM; Gibco, USA, 89% for T47D) with 10% fetal bovine serum and 1% 100 IU/ml penicillin-streptomycin. BALB/c nude mice (female, 4–5-weeks-old, 16–18 g) were acquired from SiPeiFu Biotechnology Co., Ltd. (Beijing, China). The animals were maintained in a specific pathogen-free environment with free access to food and water. New Zealand strain white rabbits (female, 2.0 ± 0.5 kg) were acquired from Beijing Huafukang Biotechnology Co., Ltd. (Beijing, China). All animal experiments were carried out 1 week after the animals adapted to the feeding environment. After evaluation and approval by the Ethics Committee of Tianjin University of Traditional Chinese Medicine, all animal experiments were conducted according to relevant procedure guidelines (Ethics Code: TCM-LAEC2022016).

2.2. Molecular docking

Molecular docking experiments were carried out in order to elucidate the interaction between the ER and phytoestrogen derived from TCM with anti-tumor effect. First, the structural formulas for phytoestrogen and estradiol were downloaded from the SciFinder website. The pre-selected ligand structure was saved in the mol2 format, and all ligands were imported into the Discovery Studio software. The minimum energy process was then performed. Second, the structures for estrogen receptors α (Erα, PDB:1QAT) and β (Erβ, PDB:3OLL) were downloaded from the Protein data bank and saved in the mol2 format. The protein structure was then imported into the Discovery Studio software. After removing the water, the binding site for the original ligand was selected, the original ligand was deleted, and each conformation was docked with ERs using the LibDock mode. Finally, the docking score was

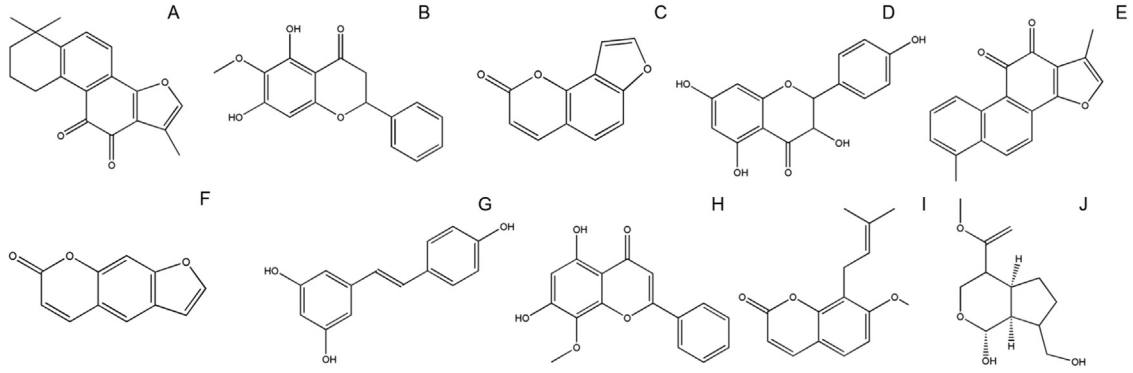

Fig. 1 – Chemical structure of phytoestrogen with anti-tumor activity. (A: Tan IIA; B: chibain A; C: isopsoralen; D: kaempferol; E: Tan I; F: psoralen; G: resveratrol; H: wogonin; I: osthole; J: genipin).

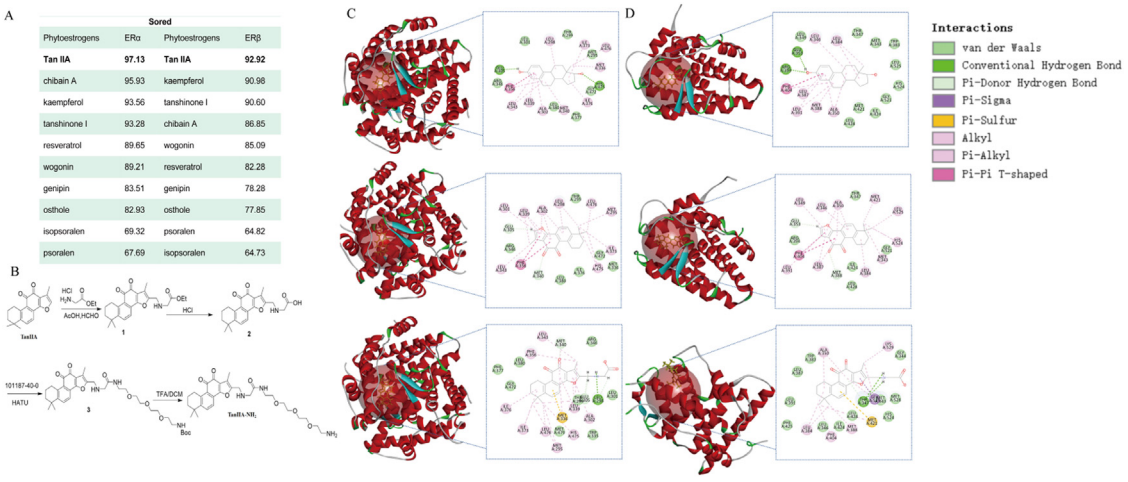

Fig. 2 – The screening and modification of Phytoestrogen-derived ligands. (A) Docking results of traditional Chinese medicine phytoestrogens and estrogen receptor under LibDock mode. (B) Synthetic route of terminal amino-modified TanIIA. Molecular docking of β-estradiol, Tan IIA and intermediate 2 with ER α protein (C) and ER β protein (D).

obtained after the program ran its course. The higher the absolute score, the stronger the hydrogen bond interaction between the ligand and ER, the closer the binding between the molecule and ER. In addition, the CDOCKER mode was used for docking verification of the bound ligands, including Tan IIA and modifiers.

2.3. *Modification of Tan IIA*

A side chain was introduced at the C16 position of Tan IIA via Mannich reaction by dissolving Tan IIA in acetic acid with glycine ethyl ester hydrochloride and formaldehyde to obtain intermediate 1 (I1; Fig. 2B). Subsequently, I1 was subjected to ester hydrolysis in hydrochloric acid to obtain intermediate 2 (I2) with a terminal carboxyl group. I2 condensation was performed to link the PEG short chain. The modification of the terminal amino group (Tan-NH_2) was thus obtained after deprotection of the protective group in trifluoroacetic acid. Detailed synthesis information is provided in the Support Information section. The chemical structure of modified Tan IIA with terminal amino group was analyzed using proton (1H) nuclear magnetic resonance spectroscopy.

2.4. *Nanoparticle preparation*

Synthesis of carboxyl-functionalized mesoporous silicon was carried out using the classical template method. Briefly, surfactant CTAB was first dissolved in deionized water. After adding ethylene glycol and ammonia water, the mixture was stirred at 60 °C for 30 min. Tetraethyl orthosilicate and 2-cyanoethyltriethoxysilane were rapidly added to the mixture under vigorous stirring for 2 h and then maintained at 60 °C for 24 h. The solution was then centrifuged at 12,000 rpm for 30 min and the pellet was washed several times with deionized water and ethanol. The dried product was functionalized with sulfuric acid at 100 °C and the template agent CTAB was removed using an acidic ethanol solution. The resulting sample was centrifuged at 12,000 rpm for 30 min and washed three times with deionized water and ethanol. The precipitate was vacuum-dried to obtain the carboxyl-functionalized mesoporous silica nanoparticles (MSN–COOH).

MSN–COOH was drug loaded using the adsorption method. Phosphate-buffered saline (PBS) buffer (pH 7.4) was utilized as the drug-carrying solvent. After adding Dox and MSN–COOH

at a drug-carrier ratio of 1:3 and stirring for 24 h, the resulting solution was centrifuged, washed twice with PBS, and dried. Dox-loaded mesoporous silica nanoparticles (Dox-MSN) were thus obtained. All supernatants and washing solutions were collected to calculate drug loading.

Dox-MSN was ultrasonically dispersed in the MES buffer (pH 6.0). Then, EDC and NHS were added and mixed well, shaken at room temperature for 1 h to activate the carboxyl groups, and centrifuged. The precipitate was then redispersed in PBS buffer (pH 7.4). After adding Tan-NH_2 and trimethylamine in the buffer, the reaction was allowed to incubate for 3 h and then centrifuged. The precipitate was washed with PBS buffer three times to obtain Tan-Dox-MSN. All supernatants and washing solutions were combined to calculate the graft ratio.

2.5. *Nanoparticle characterization*

2.5.1. *Particle size, zeta potential, and morphology*

The hydrodynamic particle size, polydispersity index (PDI) and zeta potential for MSN–COOH, Dox-MSN and Tan-Dox-MSN after ultrasonic dispersion were measured by a Zetasizer (Nano ZS; Malvern Instruments, Malvern, UK). All measurements were performed in triplicate. The morphology of MSN–COOH, Dox-MSN, and Tan-Dox-MSN was observed using a transmission electron microscope (TEM; JEOL, Tokyo, Japan) and photographed.

2.5.2. *Thermodynamic analysis*

For differential scanning calorimetry experiments (DSC, Q1000, TA Instrument, USA), samples (Dox powder, Tan-NH_2 powder, MSN–COOH, Dox-MSN, Tan-Dox-MSN, and mixture of MSN–COOH, Tan-NH_2, and Dox powder) were placed in pierced aluminum pans and heated from 30 to 300 °C at a scanning rate of 10 °C/min under nitrogen protection.

Thermogravimetric analyzer (Discovery TGA 5500, TA instruments, USA) was used to verify drug loading and grafting rates. The samples (MSN–COOH, Dox-MSN, and Tan-Dox-MSN) were placed in a platinum plate, and the temperature was raised from room temperature to 900 °C at a heating rate of 10 °C/min. The amount of sample loss was measured, while the curve was recorded, and then the temperature was lowered to room temperature.

2.6. *Hemolysis assays*

The safety of nano preparations *in vivo* was evaluated using hemolysis experiments. After removing the fiber from rabbit blood samples, normal saline was added for centrifugation, which was performed several times. The red blood cell samples were washed and diluted to a concentration of 2%. Equal volumes of 2% red blood cell suspension, normal saline (negative control), deionized water (positive control), and physiological saline solution containing different preparations were added into each tube and observed at 37 °C. Hemolysis was recorded for each tube at 1 h, 2 h, 3 h, 4 h, 5 h, 8 h and 24 h. The samples were centrifuged (1,500 rpm, 10 min) and photographed after 24 h to determine whether hemolysis and agglutination occurred. The hemolysis rate was determined using absorbance values at 540 nm that were obtained with a Microplate Reader (Spark; Tecan, Männedorf, Switzerland) using the following formula:

$$\text{Hemolysis (\%)} = [(A_1 - A_2)/(A_3 - A_2)] \times 100\%,$$

where A_1, A_2 and A_3 refer to the absorbance of different preparations, negative control, and positive control, respectively.

2.7. *Drug release*

In vitro release behavior of Dox, Dox-MSN and Tan-Dox-MSN solutions was determined using the dialysis method. The PBS buffers with different pH were selected as the release media. The dialysis bag storing 3 ml the preparation was placed in a container with 150 ml medium. The temperature was maintained at 37 ± 1 °C, and the rotational speed was set to 100 rpm. A total of 2 ml the sample were removed from the release medium after 10, 30, 60, 120, 180, 360, 480, 600, 720 and 1,440 min and then the same volume of blank release medium was added to the container. The contents of Dox filtrate were determined using the microplate reader. The release studies for each group were repeated three times.

2.8. *Cytotoxicity study*

The cytotoxicity of MSN–COOH and ligand in MCF-7, T47D, and MCF10A cells was measured using the CCK-8 kit. After the cells were cultured in a 96-well plate for 24 h, the cytotoxicity test was initiated, and the previous medium was replaced with 100 µl medium containing different concentrations of MSN–COOH and the ligand. The medium was removed after 24 h and 100 µl 10% CCK-8 diluent were added to each well. The solution was incubated at 37 °C for 1 h and the absorbance values at 450 nm were determined using a microplate reader. The cytotoxicity effect of Dox and the formulation(Dox-MSN, Tan-Dox-MSN and Tan-MSN) on MCF-7 cells was measured using same method. Cell viability (CV,%) was calculated using the following formula:

$$\text{Cell Viability (\%)} = [(A_s - A_b)/(A_c - A_b)] \times 100\%,$$

where A_b, A_c, and A_s refer to the absorbance of the blank, control, and experimental wells, respectively.

2.9. *Anti-metastasis study*

2.9.1. *Scratch wound-healing assay*

Human breast ductal carcinoma T47D cells were trypsinized and then seeded in 6-well plates with 2 ml serum-free medium per well. The center of each well in the 6-well plate was scratched with a 200-µl pipette tip, observed, and photographed under an optical microscope. Different concentrations (1, 2 and 5 µg/ml) of Tan-NH_2 and nanocarrier solutions (Tan-NH_2: 5 µg/ml, MSN–COOH: 62.5 µg/ml) were then added. After 24 h, cell healing in each group was observed under an optical microscope and photographed. Image J software was used to calculate the scratch area. The cell migration rate of the control group was 100%, which was used to calculate the test group migration rates.

2.9.2. Transwell migration and invasion assays

T47D cells were trypsinized and resuspended in serum-free medium and seeded in the upper Transwell chamber at a density of 1×10^4 cells/200 μl medium per well. In addition, 800 μl complete medium containing 10% serum were added to the lower chamber. Liquid in the upper chamber was aspirated after the cells adhered and different concentrations (1, 2 and 5 μg/ml) of Tan-NH_2 and nanocarrier solutions (Tan-NH_2 content: 5 μg/ml in Tan-MSN group) were added to the upper chamber. Each group was tested in triplicate. The samples were incubated at 5% CO_2 and 37 °C for 24 h. Liquid in the upper and lower chambers was then removed and 4% paraformaldehyde was added to fix the cells. The unmigrated cells in the upper chamber were gently wiped off with cotton balls. The cells were then stained with 1% Crystal Violet solution and photographed under an optical microscope. The migrated cells were quantitatively analyzed using a microplate reader. Specifically, they were ultrasonically treated with 35% glacial acetic acid to completely dissolve the crystal violet. Then, 200 μl the cell sample were pipetted into a 96-well plate and a microplate reader was used to measure the absorbance at 570 nm. The migration rate of the control group was 100%, which was used to calculate the migration rates of the other groups.

For the invasion assays, the PET membrane was coated with Matrigel and then the cells were cultured. The subsequent procedure was the same as that for the above migration test. After incubation for 24 h with medium containing Tan-NH_2 or nano-carrier solution of appropriate concentration, the invading cells were stained and photographed.

2.10. Cellular uptake study

2.10.1. Cellular uptake

Studying the uptake of different cells is an important aspect of investigating the targeting specificity of Tan IIA-modified MSN. The uptake of different nano formulations by MCF-7, T47D, and MCF10A cells was evaluated using a confocal laser scanning microscope (Zeiss, USA) with a 40× objective and Dox as a fluorescent probe. The quantitative analysis of Dox fluorescence intensity of cellular uptake was performed using flow cytometry (Attune, Thermo Fisher, USA). For qualitative analysis of cellular uptake, MCF-7, T47D, and MCF10A cells were seeded on round coverslips in 12-well plates. After incubation for 24 h, the cells were cultured in fresh medium containing Dox, Dox-MSN, and Tan-Dox-MSN solutions for 1.5 h. Then, 1 ml the mixture containing 1.67 μg/ml Hoechst 33342 was added to each well to stain the nuclei, and the cells were incubated in the dark at 37 °C for 30 min. After washing with PBS three times, the round coverslips were placed on the glass with anti-fluorescence attenuator for observation. MCF-7, T47D, and MCF10A cells were seeded in 6-well plates for quantitative analysis of cellular uptake. After incubation for 24 h, the cells were cultured in fresh medium containing Dox, Dox MSN and Tan Dox MSN solutions with an equivalent concentration of Dox for 1 h, 2 h or 4 h. After washing three times with PBS buffer, the cells were collected for flow cytometry analysis.

2.10.2. Cell uptake pathways

A competitive study was carried out to investigate whether the receptor ligand was effectively bound. The ligand and estrogen receptor inhibitor (ICI 182780) solutions were incubated with MCF-7 cells for 12 h before the cell uptake experiment.

To investigate the energy dependence of cell intake, MCF-7 cells were seeded in 6-well plates, incubated at 37 °C for 24 h, maintained at 4 °C for 30 min, and then incubated with Dox-MSN or Tan-Dox MSN (Dox concentration: 5 μg/ml) at 4 °C for 2 h. The quantitative analysis of cell uptake was then performed. To reveal the mechanism of cell uptake, the MCF-7 cells were incubated for 1 h at 37 °C with methyl-b-cyclodextrin (5 mmol/l), amiloride (20 μmol/l), chlorpromazine (30 μmol/l), and colchicine (250 μmol/l) prior to treatment with Dox-MSN or Tan-Dox-MSN for an additional 2 h. No inhibitor was added to the control group, and the results were expressed as the relative uptake inhibition ratio.

2.11. Tumor targeting evaluation

Breast cancer xenograft model mice were prepared to evaluate the tumor targeting of Tan IIA-modified MSN. ICG or Dox was used as a fluorescent probe. To prepare the ICG formulation, Dox was replaced with ICG using the steps described in the 'Nanoparticle preparation' section. Briefly, 0.2 ml the Matrigel cell suspension (1×10^8 MCF-7 cells/ml) were subcutaneously injected into the left side of female BALB/c nude mice. When the tumor volume increased to 100 mm^3 (tumor volume (V)=$ab^2/2$; a: tumor length, b: tumor width), the mice were randomly divided into the saline, Dox-Sol, Dox MSN, Tan-Dox MSN, ICG-Sol, and Tan-ICG-MSN groups (three mice per group, 1 mg/kg for ICG, 2 mg/kg for Dox). The ICG fluorescence intensity of each mouse was measured using a live imaging system at the excitation wavelength of 780 nm and the emission wavelength of 800 nm 1 h, 4 h, 12 h and 24 h after administration. In addition, fluorescence intensity of the main organs and tumor tissues was observed after the mice were sacrificed after 12 h of Dox administration to evaluate the distribution of Tan IIA-modified MSN *in vivo*.

2.12. Anti-tumor efficiency

Breast cancer xenograft model mice were obtained as described in the 'Tumor targeting evaluation' section. The mice were randomly divided into the saline, Dox injection, Dox-Sol, Dox-MSN, Tan-MSN, and Tan-Dox-MSN groups (five mice per group). Saline group mice were injected with 100 μl saline to serve as the control group. For the Dox injection group, 100 μl commercial Dox (2 mg/kg) were injected. For the Tan-MSN group, 100 μl carrier (same carrier mount with Tan-Dox-MSN) were injected. The other groups were injected with 100 μl per mouse (Dox: 2 mg/kg) once every 3 d, five times in total. The changes in mouse body weight and tumor volume were recorded after drug administration. Finally, mouse blood samples were collected to measure the levels of biochemical markers of cardiac function (Creatine Kinase, CK), hepatic function (Aspartate aminotransferase, AST), and renal function (Creatinine, CRE) 24 h after the last

administration. The main mouse organs and tumor tissues were also extracted and weighed.

To observe the changes in each organ, tumor-bearing mice in each group were sacrificed and weighed. The samples were dissected, and the heart, liver, spleen, lung, kidney, and other organs were taken-out and weighed. The weight ratio of the corresponding mouse before sampling served as the organ index.

2.13. *Immunohistochemistry*

The main organ samples were dehydrated, embedded in paraffin, and then stained with hematoxylin and eosin. A microscope (NIKON Eclipse Ci) was used for observation. Immunofluorescence staining was performed using a TUNEL detection kit (Roche). Tumor section slides were de-affiliated, rehydrated, and stained with DAPI.

2.14. *Statistical analysis*

All values were expressed as mean ± standard deviation (SD). Statistical significance was analyzed using one-way ANOVA or Student's t-test with Graphpad Prism 8 software, and P value<0.05, <0.01, or <0.001 indicated statistical significance.

3. Result and discussion

3.1. *Molecular docking*

Molecular docking technology has been widely used in molecular biology, pharmacology, pharmacy, and other disciplines. By simulating the interaction between the targeted receptors determined by conformation and small-molecule ligands or drugs, the binding of ligands can be evaluated, and drug targets can be predicted.

By using the LibDock mode, the structures of Tan IIA, Tan I, resveratrol, wogonin, osthole, psoralen, isopsoralen, genipin, kaempferol and chibain A are used as ligands for docking with ERs. The 10 traditional Chinese medicine phytoestrogens that were successfully docked with ER were scored, as shown in Fig. 2A. Tan IIA scored first in docking with two subtypes of ERs, so Tan IIA was preselected. The ligands were subjected to subsequent docking studies.

The modified Tan IIA with the terminal amino group (Tan-NH_2) was successfully prepared by the Mannich addition, ester hydrolysis, and condensation reactions. LCMS: RT= 0.889 min, $[M+H]^+$=556.3, purity: 95% 1H NMR (400 MHz, DMSO) δ 9.60 (s, 1H), 8.58 (t, J = 5.5 Hz, 1H), 7.87 (d,J = 8.2 Hz, 3H), 7.60 (d,J = 8.1 Hz, 1H), 4.35 (s, 2H), 3.78 (s, 2H), 3.62 – 3.49 (m, 11H), 3.43 (t,J = 5.6 Hz, 2H), 3.28 (dd,J = 11.0, 5.4 Hz, 2H), 3.09 (t,J = 6.0 Hz, 2H), 2.98 (dd,J = 10.5, 5.2 Hz, 2H), 2.22 (s, 3H), 1.79 – 1.57 (m, 4H), and 1.29 (s, 6H).

The preselected active ingredient ligands of traditional Chinese medicine were docked with the ER protein by the CDOCKER mode, and to compare the binding effect, the original ligands β-estradiol and α-estradiol were docked with the ER protein by CDOCKER. The results showed that both Tan IIA and its terminal carboxyl-modified products could be successfully docked. The -CDOCKER INTERACTION ENERGY between Tan IIA modifications and ER was shown in Table S1–S2, while the lower the energy, the better the stability, indicating that Tan IIA and its modifications are relatively stable when binding to ER-α and ER-β.

As shown in Fig. 2C, Tan IIA and intermediate 2 form hydrogen bond, hydrophobic, Pi-sulfur and Pi-Sigma interactions. As shown in Fig. 2D, Tan IIA and intermediate 2 form hydrogen bond, hydrophobic and Pi-sulfur interactions with amino acid residues in ER-β.

Tan IIA has a wide range of pharmacological activities; however, its strong lipophilicity, low bioavailability and short half-life prompt researchers to modify its structure to improve its physicochemical properties and pharmacokinetic parameters. At present, four main modification sites for Tan IIA are identified, namely, the 1-position of the A ring, ortho-diquinone of the C-ring, methyl group of the 18-position of the D-ring, and 16-position of the D-ring. The substitution reaction occurs at C at the 1-position of the A ring, and the subsequent reaction occurs after bromine substitution to obtain hydroxyl, alkoxy, and monosaccharide-substituted derivatives, improving solubility and biological activity. By using the o-diquinone structure of the C ring, it can react with primary amines or aromatic primary amines in ethanol at room temperature to obtain a nitrogen-containing five-membered ring. However, some studies have shown that after the modification at the o-diquinone site, its activity decreased, indicating that the key site of Tan IIA cytotoxicity may be the ortho-diquinone structure of the C ring. Another study showed that various imidazole derivatives were obtained by modifying the o-diquinone structure of Tan IIA, and one of them had an obvious inhibitory effect on breast cancer MDA-MB-231 and a certain effect. Tan IIA derivatives provide a basis for the prevention of cancer metastasis [26]. The methyl group at the 18-position of the furan ring of the D-ring can be oxidized to a hydroxyl group, and the 16-position is the most active reactive site, which can be used for sulfonation, Vilsmeier reaction, Mannich reaction, etc. Tan IIA sodium sulfonate obtained by sulfonation is used as a commercial preparation for the treatment of coronary heart diseases, angina pectoris, venous embolism, and other diseases.

3.2. *Characterization of nanoparticle*

The physicochemical properties of MSN–COOH, Dox-MSN, and Tan-Dox-MSN are summarized in Table S3. All NPs demonstrated a narrow size distribution (PDI < 0.3) with sizes ranging from 110 to 150 nm. The zeta potential of Dox-MSN and Tan-Dox-MSN was approximately −20 mV, suggesting a change during the process of drug loading and ligand modification, shifting from a negative potential to a positive potential. From the TEM results (Fig. 3A), the nanoparticles are spherical, with good dispersibility, round shape and uniform particle size distribution. Surface-modified tumor-targeting ligands have little effect on the morphology and particle size of nanoparticles.

From the DSC analysis (Fig. S2), the preparation contains drugs and ligands. The endothermic peaks of Dox and Tan-NH_2 are located at 242 °C and 218 °C, respectively. Although the endothermic peaks of Tan-NH_2 in the physical mixing

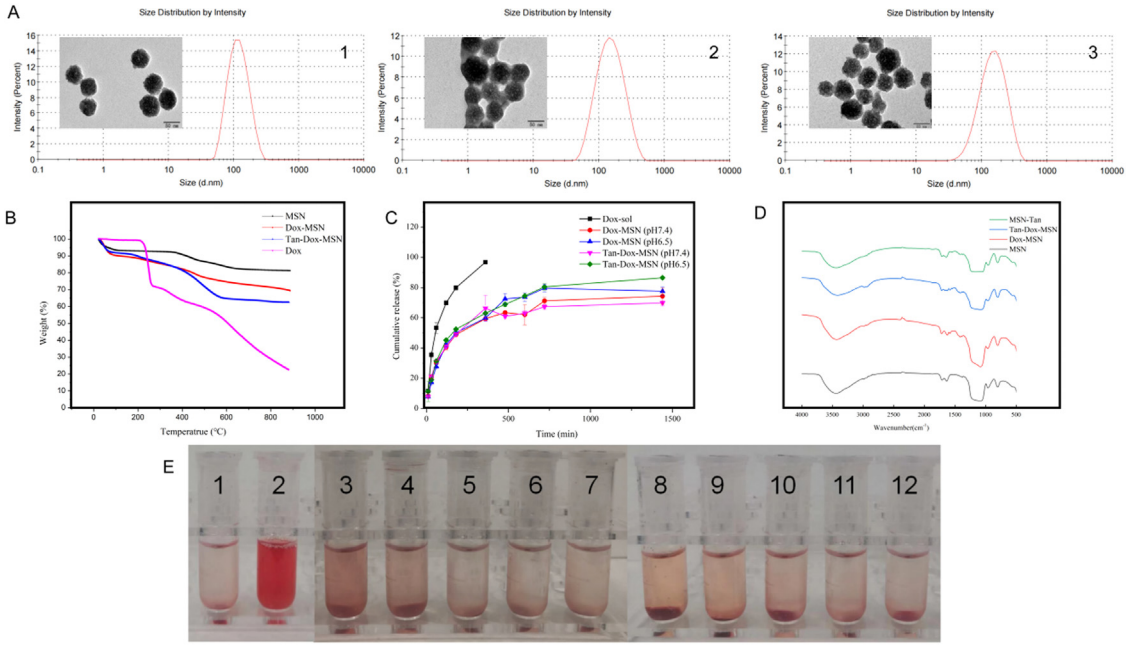

Fig. 3 – Characterization and safety evaluation of nanoparticles. (A) TEM and DLS results of MSN–COOH (1), Dox-MSN(2), Tan-Dox-MSN(3); (B) Thermogravimetric Analysis Results; (C) *In vitro* release profiles of Dox in different formulations (mean ± SD, $n = 3$); (D) FTIR spectra of Tan-MSN, Tan-Dox-MSN, Dox-MSN, and MSN–COOH; (E) Hemolysis experiments of different preparations (1: normal saline; 2: deionized water; 3–7: Dox-MSN 4000–20 μg/mL; 8–12: Tan-Dox-MSN 4000–20 μg/ml).

group are not apparent, the absorption of Dox can still be observed. Thermal peaks and each group of preparations did not respond at the corresponding melting temperature. This result indicates that Dox and Tan-NH_2 were successfully loaded on MSN and may exist in the nanoparticles as an amorphous or solid solution on the surface or pores.

By the thermogravimetric analysis of MSN–COOH, Dox-MSN, and Tan-Dox-MSN, the results are shown in Fig. 3B. The weight loss below 200 °C occurs following a high-temperature removal of water molecules adsorbed on the surface of nanoparticles, and 200–900 °C is the weight loss of organic groups. According to the data analysis, Dox-MSN has a weight loss of 12.02% compared with MSN–COOH; thus, the dosage of Dox loaded in MSN–COOH is ~12.02%, which is consistent with the previous high-performance liquid chromatography results, indicating that mesoporous silicon is the perspective load carrier for Dox. Moreover, according to the weight loss rate of Tan-Dox-MSN, Tan-NH_2 was successfully modified on the mesoporous silicon support. Compared with MSN–COOH, the weight loss was 18.86%, and the grafting rate was 6.84%, which was lower than that of liquid phase determination. The obtained grafting rate was due to drug loss during the modification process of Tan-Dox-MSN.

Infrared spectroscopy was used to characterize MSN and different formulations (Fig. 3); the results show that the typical peaks of MSN–COOH appear at 1084 and 798 cm^{-1}, which are the characteristic peaks of Si-O-Si stretching vibration [27]. In addition, the infrared spectrum of the MSN–COOH sample has a peak at 1718 cm^{-1}, which is the stretching vibration frequency of C=O in the carboxyl group. After loading Dox in Dox-MSN, a new peak of DOX molecular ring breathing vibration appeared at 1581 cm^{-1}. New peaks in Tan-Dox-MSN and Tan-MSN appeared at 1550 cm^{-1} after modification with Tan-NH_2, which belonged to the bending vibration peaks of N–H. The results showed that the Tan-Dox-MSN payload was loaded with Dox and Tan-NH_2.

3.3. *Hemolysis assays*

As shown in Fig. 3E, the solution in the deionized water group was clear red, and the remaining tubes did not appear as clear red within 24 h. When each preparation group contained 20–4,000 μg per 2 ml, a clear red appearance was not observed, indicating that the preparation was in a wider range. It has good biocompatibility and blood safety within the concentration range.

3.4. *Drug release*

As shown in Fig. 3C, the cumulative-release rate of the Dox solution group in the pH 7.4 buffer for 6 h was (96.81% ± 0.60%), and the release was complete, whereas the Dox-MSN group and the Tan-Dox-MSN group showed sustained release effect in both buffers, and in PBS buffer of pH 6.5 simulating the tumor microenvironment, the cumulative release rate at 24 h was higher than that in PBS buffer of pH 7.4 simulating body fluids, indicating that the MSN group and the Tan-Dox-MSN group had certain pH response characteristics of the tumor microenvironment.

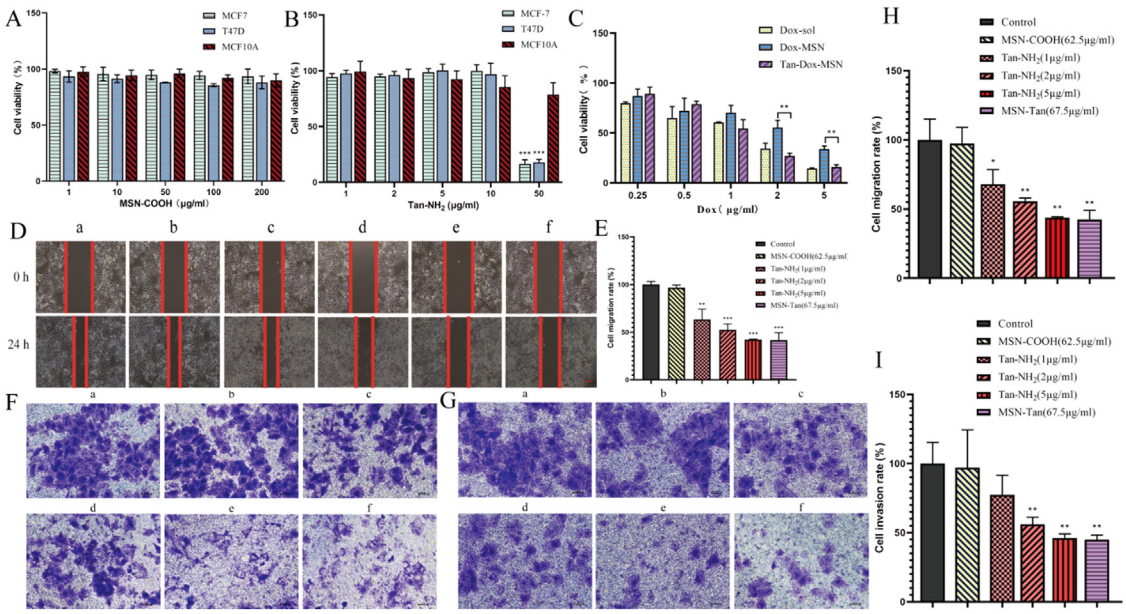

Fig. 4 – Cytotoxicity and *in vitro* inhibitory effects of Tan-NH_2 and carrier on cell migration. (A) Cytotoxicity of MSN–COOH on MCF-7, T47D and MCF10A cells; (B) Cytotoxicity of Tan-NH_2 on MCF-7, T47D and MCF10A cells (*$P<0.001$, mean ± SD, $n = 3$); (C) Cytotoxicity of preparations on MCF-7 cell; (D) Typical images of scratch wound-healing assays, scale bar: 100 μm; (E) The statistical results of scratch wound-healing assays, scale bar: 100 μm; (F) Transwell migration assay on T47D cell; (G) Transwell invasion assay on T47D cell; (H) The statistical results of Transwell migration assay; (I) The statistical results of Transwell invasion assay (*$P<0.05$, **$P<0.01$, mean ± SD, $n = 3$).**

3.5. *Cytotoxicity*

The cytotoxicity of MSN–COOH on human breast cancer (MCF-7 cells), human breast ductal carcinoma (T47D cells), and human normal breast (MCF10A cells) was determined by the CCK-8 method (Fig. 4A). In the concentration range of 1–200 μg/ml, the survival rates of the three cells were all > 85%, indicating that MSN–COOH had no significant toxicity to the three cells, and the interference of carrier toxicity could be excluded in subsequent studies.

Since Tan IIA has certain cytotoxicity to MCF-7 and T47D cells, the cytotoxicity of Tan-NH_2 to the three cells needs to be investigated. The cytotoxicity of Tan-NH_2 at a higher dose was investigated (Fig. 4B). In the concentration range of 1–50 μg/ml, the survival rate of MCF10A cells varies with the ligand. The ligand has no significant toxicity to normal cells with the increased concentration. At a higher dose of 50 μg/ml, Tan-NH_2 significantly inhibited the growth of tumor cells, the survival rate of MCF-7 cells was only 16.53%, and the survival rate of T47D cells was 17.92%. At low doses, it did not tend to promote tumor cell growth, indicating that the ligand has a certain antitumor effect, and it did not promote tumor cell growth in the concentration range of 1–50 μg/ml.

As shown in Fig. 4C, the three preparations had dose-dependent cytotoxicity. At higher concentrations, the cytotoxicity of the modified group is stronger than that of the unmodified group, which may be due to the increased cellular uptake, whereas the cell survival rate of the solution group was lower, indicating that Dox was more cytotoxic, and biocompatibility was improved after being prepared into a nanoformulation.

3.6. *Anti-metastasis study*

The higher the cell migration rate, the greater the likelihood of cancer metastasis. Compared with estrone and estradiol, which have the risk of promoting cancer metastasis, some studies have reported that Tan IIA inhibits the migration of various tumor cells. The cytotoxicity results showed that Tan-NH_2 concentration of < 10 μg/ml did not affect the activity of T47D cells. Thus, we investigated the effect of Tan-NH_2 on T47D cell migration. Accordingly, 1 μg/ml Tan-NH_2 could significantly delay the process of cells entering the central wound ($P < 0.01$), and the inhibitory ability was stronger with the increase in ligand concentration. As shown in Fig. 4D, the cells in the control group migrated to the central wound area continuously within 24 h, and the cells on both sides nearly healed, whereas the groups containing ligands could effectively inhibit the migration of tumor cells. Moreover, the MSN–COOH group inhibited migration, but the Tan-MSN group was like the solution group and strongly inhibited the migration of T47D cells.

As shown in Fig. 4F, T47D cells were treated with different concentrations of Tan-NH_2, the cell migration rate was inversely proportional to the concentration, MSN–COOH nanocarriers had little effect on cell migration, and Tan-MSN nanocarriers had good anti-cell migration effect. According to the quantitative analysis results (Fig. 4H), the cell migration rates of different concentrations of ligand solutions, *i.e.*, 1, 2,

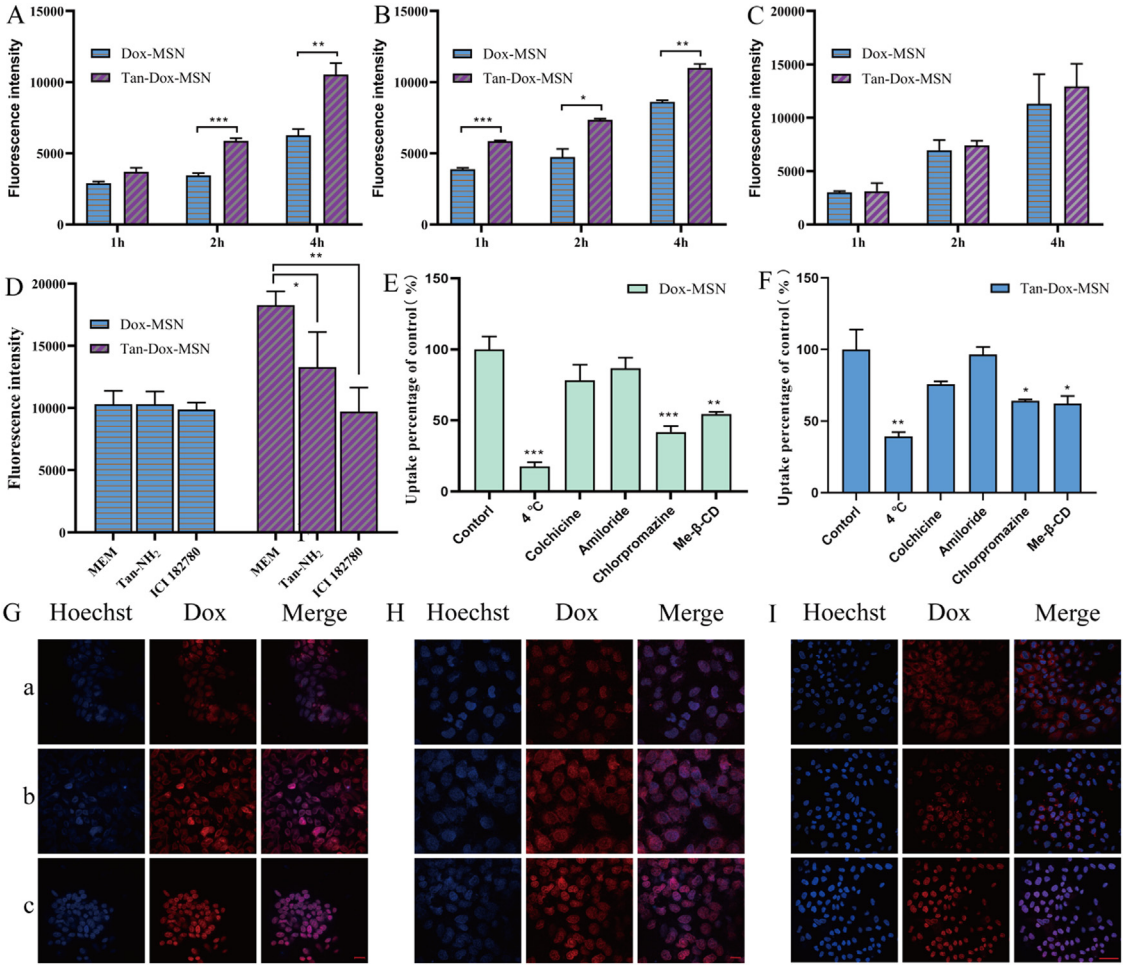

Fig. 5 – Cellular uptake of Nanoparticles. Quantitative analysis of nanoparticle uptake by MCF-7(A), T47D (B), MCF10A (C) cells incubated for different times (*$P<0.05$, $P<0.01$, ***$P<0.001$, mean ± SD, $n = 3$); (D) Uptake of different formulations in MCF-7 cells pretreated with estrogen receptor inhibitors and free ligands (**$P<0.01$, *$P<0.05$, mean ± SD, $n = 3$); Confocal images of MCF-7(E), T47D(F), MCF10A(G) incubated with Dox-sol(a), Dox-MSN(b), Tan-Dox-MSN(c) for 2 h, scale bar: 50 μm; Effects of specific endocytosis inhibitors on the uptake of Dox-MSN(H) and Tan-Dox-MSN(I) by MCF-7 cells (***$P<0.001$, **$P<0.01$, *$P<0.05$, *vs* Control, mean ± SD, $n = 3$).**

and 5 μg/ml, decreased to 63.4%, 52.6% and 42.2%, respectively, compared with the control group. In addition, compared with the control group, Tan-MSN nanocarriers containing 5 μg/ml targeting ligand had a cell migration inhibition rate of 41.6%, which could significantly inhibit the migration of T47D cells. As shown in Fig. 4G, Tan-NH_2 can dose-dependently inhibit the invasion of T47D cells. Compared with the control group, after treatment with different concentrations of the ligand solution (1, 2 and 5 μg/ml) and Tan-MSN (5 μg/ml Tan-NH_2), the cell invasion inhibition rates in each group were 77.4% and 56.1%, 46.1% and 45.0%, respectively, indicating that targeting ligands do not promote cell metastasis and have a certain inhibitory effect on tumor metastasis.

3.7. *Cellular uptake*

As shown in Fig. 5E, Dox can be used as a fluorescent probe to well indicate the cell uptake status. After incubation with MCF-7 cells for 2 h, the fluorescence intensity of the solution group was the highest, indicating that Dox can pass through the cell membrane by passive diffusion. Meanwhile, the fluorescence intensity of the Tan-Dox-MSN group was higher than that of the Dox-MSN group, which may be caused by ER overexpression in MCF-7 cells. As the uptake of MCF-7 cells, after incubation with T47D cells for 2 h, the uptake of the Dox solution group was higher than that of the preparation group, indicating that the solution group could pass through the cell membrane well through passive diffusion and could be taken up by T47D cells. The Dox signal in the solution group co-localized well with the signal of the nucleus after Hochest staining, indicating that the Dox solution at the cellular level could reach the nucleus and exert its medicinal effect. In the cell uptake experiment of NIH-3T3, the fluorescence intensity of the Tan-Dox-MSN group did not show marked signal enhancement compared with the Dox-MSN group, which may be due to the lower expressions of ERs in NIH-3T3 cells. This result shows that the nanodelivery system had little effect on the uptake of normal cells expressing ERs.

The uptake levels of the modified preparations with Tan IIA in MCF-7 (Fig. 5A) and T47D (Fig. 5B) cells were higher than those in the unmodified group at 1, 2 and 4 h, and a significant difference in the cellular intake was found at 2 and 4 h, indicating that the cellular internalization efficiency of Tan-Dox-MSN was higher than that of Dox-MSN. In MCF10A cells (Fig. 5C), no significant difference was found in the uptake of Tan IIA-modified preparations compared with the unmodified group. However, the fluorescence intensity of the cell uptake is higher, which may be related to the cell state and cell membrane fluidity.

3.8. *Cell uptake pathways*

As shown in Fig. 5D, the cellular uptake of the Tan-Dox-MSN group was significantly decreased after the addition of ICI 182780, which indicated that ERs were involved in the cellular uptake of Tan-Dox-MSN. Furthermore, upon the addition of the ligand solution, the cellular uptake was reduced and significantly different from that in the control group, suggesting that the uptake of Tan-Dox-MSN is related to Tan IIA modification. Moreover, under the same conditions, the uptake of Dox-MSN by MCF-7 cells slightly decreased after incubation with ER inhibitor, and no statistical difference was found.

The endocytic pathway of the formulations was investigated by changing the temperature and using chemical inhibitors. As shown in Fig. 5H–5I, decreasing the temperature from 37 °C to 4 °C inhibited the uptake levels of Dox-MSN and Tan-Dox-MSN by MCF-7 cells by 83.3% and 60.7%, respectively. These results indicate that the uptake of Dox-MSN and Tan-Dox-MSN is an energy-dependent endocytosis process, and ER-mediated endocytosis is an energy-dependent process. The endocytosis of the formulation was significantly inhibited by chlorpromazine and to a lesser extent by methyl-β-cyclodextrin, suggesting that the uptake process is a clathrin-dependent and cholesterol-related uptake pathway. Amiloride and colchicine had little effect on the endocytosis of the preparation, indicating that the endocytoses of Dox-MSN and Tan-Dox-MSN do not belong to macropinocytosis and are less related to actin polymerization.

3.9. *Tumor targeting evaluation*

The biodistribution of near-infrared fluorescent dye ICG-labeled nanoparticles in tumor-bearing nude mice at 1, 4, 12 and 24 h was investigated by IVIS small animal *in vivo* imager, targeting the advantages of nanoparticles *in vivo*. The excitation and emission wavelengths of the ICG dye were 780 nm and 800 nm, respectively. The colored scale was used to measure the fluorescence intensity, from dark blue to white, representing a gradual increase. Experiments were conducted by tail vein injection in the normal saline, ICG solution, ICG-MSN, and Tan-ICG-MSN groups. After administration, the fluorescence signal weakened with time, indicating that the preparations in each group could be effectively metabolized by the body.

As presented in Fig. 6A, no fluorescence was noted in the tumor site of the ICG solution group, indicating that the drug solution has no tumor-targeting property. In addition, no fluorescence signal was detected after 12 h, indicating that the ICG solution was quickly metabolized by the body and had a short half-life *in vivo*. In the ICG-MSN group, no fluorescence at the tumor site was observed at 1 and 4 h, and over time, a small amount of fluorescence at the tumor site was found at 12 h, indicating that the drug could be delivered to the tumor site by a small amount of MSN. The nanoformulation still has a certain degree of fluorescence signal at 12 and 24 h, which reflects the long-circulation advantage of the nanoformulation. The Tan-ICG-MSN group has stronger fluorescence at the tumor site than the ICG-MSN group over time, indicating that the drug can be sustained by Tan-MSN through long circulation and active targeting delivered to the tumor site.

Since Dox is mainly metabolized by the liver and excreted through the gallbladder, Fig. 6B shows that the Dox solution group still exhibited apparent fluorescence in the liver, low fluorescence in the kidney, and absence of fluorescence in the tumor site 12 h after administration in the Dox solution group, indicating that the drug solution has no tumor-targeting effect. In the Dox-MSN group, in addition to the strong fluorescence intensity in the liver, low fluorescence was noted in the lung and kidney, indicating that the drug-loaded MSN played a long-term circulation effect on the body and accumulated in small amounts in metabolic organs such as the liver and kidney. The Dox-MSN group showed apparent fluorescence at the tumor site, indicating that the nanoformulation can be passively targeted to the tumor site through the EPR effect in animal models. The tissue distribution of the Tan-Dox-MSN group was similar with that of the Dox-MSN group, indicating that the drug delivered by MSNs into the body has a long-circulating effect and accumulated in small amounts in the liver, kidney, and other metabolic organs, and in the tumor site of the Tan-Dox-MSN group, a strong fluorescence can be seen, indicating that after Tan IIA modification, the ER is overexpressed in the tumor site, which has an active targeting effect. Active targeting is stronger than passive targeting, and it has the potential to improve the therapeutic effect of the targeted drug delivery system.

3.10. *Antitumor efficiency*

As shown in Fig. 7B–7C, the inhibition of the tumor weight corresponded to the results of the tumor volume change. The tumor growth inhibition rate in the Dox-MSN group was not significantly different from the relative tumor mass and the Dox injection group, and the tumor volume and tumor weight inhibition rates were $>$ 40%, indicating that Dox-MSN can inhibit tumor growth to a certain extent effect. Owing to the lower content of Tan-NH_2 in Tan-MSN, the carrier group did not show a strong antitumor effect. The tumor growth inhibition rate of the Tan-Dox-MSN group was very high, and the relative tumor mass was significantly different from that of the Dox injection group (positive drug group) and the Dox-MSN group ($P < 0.01$), and the tumor volume and weight were inhibited The rate is $>$ 70%, indicating that the tumor-targeted modified MSNs can improve the tumor targeting of the drug, induce the accumulation of the drug-loaded nanoparticles at the tumor site, improve drug bioavailability, and improve the

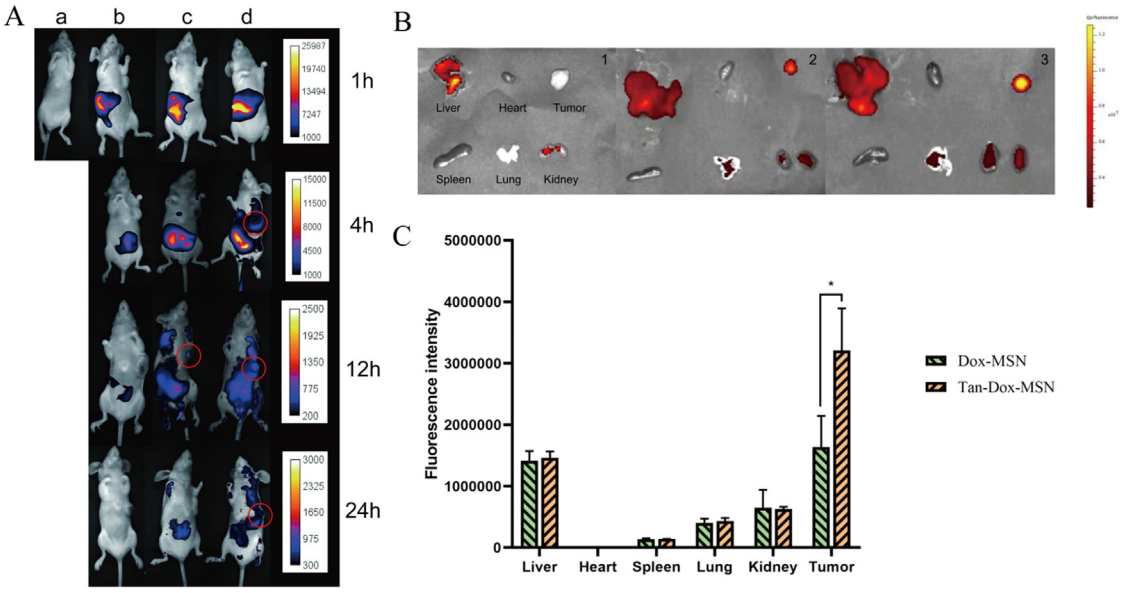

Fig. 6 – *In vivo* targeting ability evaluation. (A) ICG Fluorescence distribution in tumor-bearing nude mice at different time (a:NS;b:ICG-Sol;c:ICG-MSN;d:Tan-ICG-MSN); (B) Fluorescence distribution of main organs and tumor tissues *in vitro* in tumor-bearing nude mice for 12 h (1: Dox-sol;2:Dox-MSN;3:Tan-Dox-MSN); (C) Dox fluorescence quantitative analysis of main organs and tumor tissues of tumor-bearing nude mice for 12 h (*$P<0.05$, mean ± SD, $n = 3$).

antitumor effect *in vivo*, which indicated that Tan-Dox-MSN is a potential delivery system for antitumor drugs.

The hematoxylin-eosin staining results (Fig. S3) showed that the Tan IIA-modified MSN group did not cause significant pathological changes in various organs, indicating that nanocarriers did not show significant systemic toxicity. Compared with the organ index in the normal saline group, the index in the Dox solution, Dox-MSN, Tan-MSN, and Tan-Dox-MSN groups did not differ significantly, which preliminarily showed that the prepared preparation had low toxicity to these four organs and had good safety (Fig. S4). The potential toxicity of different preparations was further evaluated by measuring the serum AST, CRE, and CK levels.

AST activity in the serum of mice 12 d after administration was measured, and the damage level of each group of drugs on the liver was evaluated. As presented in Fig. 7D, compared with the levels in the normal saline group, the AST levels in the serum of the Dox injection and Dox solution groups were significantly increased, indicating that the groups had liver damage, which may be related Dox hepatotoxicity [28]. The AST levels in the Dox-MSN and Tan-Dox-MSN groups did not increase significantly, which may be due to the improved distribution of Dox in the body and reduced damage to the liver after the adsorption of Dox by MSNs. The circulating amount of free CRE in the serum depends entirely on its excretion level; thus, free CRE in the serum can be quantified for renal function detection. High CRE levels are observed with decreased excretion in chronic renal failure and acromegaly. Studies have shown that Dox can lead to nephrotic syndrome, resulting in high CRE levels in the serum [29]. The CRE levels in the serum of mice 12 d were measured after administration, and the effects of each group of drugs on kidney damage were evaluated. As presented in Fig. 7E, compared with the positive drug group (Dox injection), the CRE levels in the serum of the Dox solution, Dox-MSN and Tan-Dox-MSN groups were high, indicating that the preparation caused a certain degree of kidney damage. Moreover, the CRE level in the serum of the Tan-Dox-MSN group was lower than that of the Dox-MSN group, suggesting that the nanoparticles modified with Tan IIA can reduce the toxicity of the drug to the kidneys to a certain extent. CK is widely present in skeletal, cardiac, and smooth muscles. When muscle cells are damaged, the CK activity in the serum increases [28]. CK activity in the serum of mice 12 d after administration was measured, and the effects of each group of drugs on muscle cells were evaluated, focusing on the damage to myocardial cells. As shown in Fig. 7F, compared with the activity in the normal saline group, the CK activity in the serum of the Dox-MSN, Tan-MSN and Tan-Dox-MSN groups did not change significantly, indicating the lack of obvious muscle cell damage. Compared with the activity in the normal saline group, the CK activity in the serum of the Dox injection and Dox solution groups was significantly increased, indicating that Dox has significant cardiotoxicity.

3.11. *Immunohistochemistry analysis*

Subsequently, an immunofluorescent TUNEL staining assay was applied to investigate tumor cell apoptosis. As shown in Fig. 7G, compared with normal saline, the number of green positive nuclei in the Dox injection, Dox solution, Dox-MSN and Tan-Dox-MSN groups increased, indicating that these groups significantly promoted the apoptosis of MCF-7 cells.Compared with the number of green nuclei in the Dox solution group, the number in the Dox-MSN and Tan-Dox-MSN groups increased, indicating that the targeted modification of mesoporous silicon nanoparticles and Tan IIA

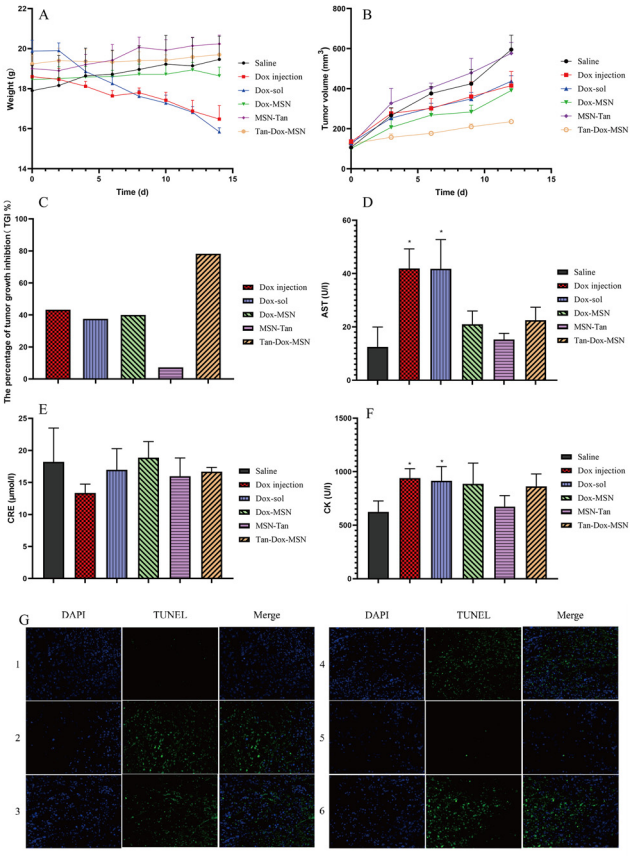

Fig. 7 – *In vivo* anti-tumor study of Dox in mice. (A) Weight-time change of mice after administration; (B) Tumor volume-time changes of mice after administration; (C) Tumor growth inhibition rate in different group of mice; (D) AST levels in serum of mice in different groups (*$P<0.05$ vs Saline); (E) CRE levels in serum of mice in different groups; (F) CK levels in serum of mice in different groups (*$P<0.05$ vs Saline); (G) Tumor tissue apoptosis in different group of mice (x 200, 1:Saline;2:Dox Injection;3:Dox-sol;4:Dox-MSN;5:Tan-MSN;6:Tan-Dox-MSN)).

nanoparticles can effectively deliver drugs to the tumor site and significantly promote the apoptosis of MCF-7 cells.

4. Conclusion

In this study, the affinity of the active ingredients of traditional Chinese medicine with estrogen-like effects to ERs was verified by molecular docking technology, and Tan IIA with a better binding effect was screened out as a preselected ligand. The modified Tan IIA with a terminal amino group (Tan-NH_2) was successfully prepared. Tan-NH_2 showed good biosafety, tumor targeting, and antitumor and antitumor metastasis effect. Tan-Dox-MSN as a novel phytoestrogen-modified nanoparticle had uniform particle size, good dispersibility, and high drug-loading capacity. Tan-Dox-MSN has better targeting ability and antitumor effect and lower toxicity to normal organs through *in vivo* and *in vitro* validation. Our confirmatory research shows that MSN Tan can be a promising drug delivery platform for the treatment of diseases with ER overexpression characteristics, such as breast cancer.

Conflicts of interest

The authors declare that there is no conflicts of interest.

Acknowledgement

This work was supported by the Tianjin University of Traditional Chinese Medicine Scientific Research Project for the New Teacher [grant number: XJS2022212]; The Science and Technology Program of Tianjin [grant number: 21YJDJC00020]; The Science and Technology Project of Haihe Laboratory of Modern Chinese Medicine [grant number: 22HHZYSS00005].

Supplementary materials

Supplementary material associated with this article can be found, in the online version, at doi:10.1016/j.ajps.2023.100827.

References

[1] Siegel RL, Miller KD, Fuchs HE, Jemal A. Cancer statistics, 2022. CA Cancer J Clin 2022;72(1):7–33.
[2] Wicki A, Witzigmann D, Balasubramanian V, Huwyler J. Nanomedicine in cancer therapy: challenges, opportunities, and clinical applications. J Control Release 2015;200:138–57.
[3] Danhier F. To exploit the tumor microenvironment: since the EPR effect fails in the clinic, what is the future of nanomedicine? J Control Release 2016;244(Pt A):108–21.
[4] Ju X, Chen H, Miao T, Ni J, Han L. Prodrug delivery using dual-targeting nanoparticles to treat breast cancer brain metastases. Mol Pharm 2021;18(7):2694–702.
[5] Guo Q, Zhu Q, Miao T, Tao J, Ju X, Sun Z, et al. LRP1-upregulated nanoparticles for efficiently conquering the blood-brain barrier and targetedly suppressing multifocal and infiltrative brain metastases. J Control Release 2019;303:117–29.
[6] Ni J, Miao T, Su M, Khan NU, Ju X, Chen H, et al. PSMA-targeted nanoparticles for specific penetration of blood-brain tumor barrier and combined therapy of brain metastases. J Control Release 2021;329:934–47.
[7] Khan NU, Ni J, Ju X, Miao T, Chen H, Han L. Escape from abluminal LRP1-mediated clearance for boosted nanoparticle brain delivery and brain metastasis treatment. Acta Pharm Sin B 2021;11(5):1341–54.
[8] Davis ME, Chen ZG, Shin DM. Nanoparticle therapeutics: an emerging treatment modality for cancer. Nat Rev Drug Discov 2008;7(9):771–82.
[9] Osborne CK, Yochmowitz MG, Knight WA, McGuire WL. The value of estrogen and progesterone receptors in the treatment of breast cancer. Cancer 1980;46(12 Suppl):2884–8.
[10] Ali S, Buluwela L, Coombes RC. Antiestrogens and their therapeutic applications in breast cancer and other diseases. Annu Rev Med 2011;62:217–32.
[11] Sun HB, Zheng Y, Ou W, Fang Q, Li P, Ye X, et al. Association between hormone receptor expression and epidermal growth factor receptor mutation in patients

operated on for non-small cell lung cancer. Ann Thorac Surg 2011;91(5):1562–7.
[12] Liu J, Chen G, Meng XY, Liu ZH, Dong S. Serum levels of sex hormones and expression of their receptors in thyroid tissue in female patients with various types of thyroid neoplasms. Pathol Res Pract 2014;210(12):830–5.
[13] Rosen ST, Maciorowski Z, Wittlin F, Epstein AL, Gordon LI, Kies MS, et al. Estrogen receptor analysis in chronic lymphocytic leukemia. Blood 1983;62(5):996–9.
[14] Mamnoon B, Feng L, Froberg J, Choi Y, Sathish V, Mallik S. Hypoxia-responsive, polymeric nanocarriers for targeted drug delivery to estrogen receptor-positive breast cancer cell spheroids. Mol Pharm 2020;17(11):4312–22.
[15] Tang H, Chen J, Wang L, Li Q, Yang Y, Lv Z, et al. Co-delivery of epirubicin and paclitaxel using an estrone-targeted PEGylated liposomal nanoparticle for breast cancer. Int J Pharm 2020;573:118806.
[16] Dreaden EC, Mwakwari SC, Sodji QH, Oyelere AK, Ei-Sayed MA. Tamoxifen-poly(ethylene glycol)-thiol gold nanoparticle conjugates: enhanced potency and selective delivery for breast cancer treatment. Bioconjug Chem 2009;20(12):2247–53.
[17] Mamnoon B, Feng L, Froberg J, Choi Y, Sathish V, Taratula O, et al. Targeting estrogen receptor-positive breast microtumors with endoxifen-conjugated, hypoxia-sensitive polymersomes. ACS Omega 2021;6(42):27654–67.
[18] Vazquez Rodriguez G, Abrahamsson A, Jensen LD, Dabrosin C. Estradiol promotes breast cancer cell migration via recruitment and activation of neutrophils. Cancer Immunol Res 2017;5(3):234–47.
[19] Salmaso V, Moro S. Bridging molecular docking to molecular dynamics in exploring ligand-protein recognition process: an overview. Front Pharmacol 2018;9:923.
[20] Ballante F, Kooistra AJ, Kampen S, de Graaf C, Carlsson J. Structure-based virtual screening for ligands of G protein-coupled receptors: what can molecular docking do for you? Pharmacol Rev 2021;73(4):527–65.
[21] Bai Z, Gust R. Breast cancer, estrogen receptor and ligands. Arch Pharm 2009;342(3):133–49.
[22] Warner M, Huang B, Gustafsson JA. Estrogenreceptor beta as a pharmaceutical target. Trends Pharmacol Sci 2017;38(1):92–9.
[23] Duffy C, Perez K, Partridge A. Implications of phytoestrogen intake for breast cancer. CA Cancer J Clin 2007;57(5):260–77.
[24] Dutta S, Kharkar PS, Sahu NU, Khanna A. Molecular docking prediction and *in vitro* studies elucidate anti-cancer activity of phytoestrogens. Life Sci 2017;185:73–84.
[25] Bi Z, Wang Y, Zhang W. A comprehensive review of tanshinone IIA and its derivatives in fibrosis treatment. Biomed Pharmacother 2021;137:111404.
[26] Wu Q, Zheng K, Huang X, Li L, Mei W. Tanshinone-IIA-based analogues of imidazole alkaloid act as potent inhibitors to block breast cancer invasion and metastasis *in vivo*. J Med Chem 2018;61(23):10488–501.
[27] Sun K, You C, Wang S, Gao Z, Wu H, Tao WA, et al. NIR stimulus-responsive core-shell type nanoparticles based on photothermal conversion for enhanced antitumor efficacy through chemo-photothermal therapy. Nanotechnology 2018;29(28):285302.
[28] Song S, Chu L, Liang H, Chen J, Liang J, Huang Z, et al. Protective effects of dioscin against doxorubicin-induced hepatotoxicity via regulation of Sirt1/FOXO1/NF-κb signal. Front Pharmacol 2019;10:1030.
[29] Boonsanit D, Kanchanapangka S, Buranakarl C. L-carnitine ameliorates doxorubicin-induced nephrotic syndrome in rats. Nephrology 2006;11(4):313–20.